Microwave interference from a spin ensemble and its mirror image in waveguide magnonics

B.-Y. Wu,[1,*] Y.-T. Cheng,[1,*] K.-T. Lin,[2,*] F. Aziz,[1,3] J.-C. Liu,[4] K.-V. Rangdhol,[1] Y.-Y. Yeung,[1] Sen Yang,[5] Qiming Shao,[4] Xin Wang,[1] G.-D. Lin,[2,6,7] Franco Nori,[8,9] and I.-C. Hoi[1,†]

[1] *Department of Physics, City University of Hong Kong, Kowloon, Hong Kong SAR, China*
[2] *Department of Physics and Center for Quantum Science and Engineering, National Taiwan University, Taipei 10617, Taiwan*
[3] *Department of Physics, National Tsing Hua University, Hsinchu 30013, Taiwan*
[4] *Department of Electronic and Computer Engineering, The Hong Kong University of Science and Technology, Clear Water Bay, Kowloon, Hong Kong SAR, China*
[5] *Department of Physics and IAS Center of Quantum Technologies, The Hong Kong University of Science and Technology, Clear Water Bay, Kowloon, Hong Kong SAR, China*
[6] *Physics Division, National Center for Theoretical Sciences, Taipei 10617, Taiwan*
[7] *Trapped-Ion Quantum Computing Laboratory, Hon Hai Research Institute, Taipei 11492, Taiwan*
[8] *Center for Quantum computing, and Cluster for Pioneering Research, RIKEN, Wakoshi, Saitama 351-0198, Japan*
[9] *physics Department, The University of Michigan, Ann Arbor, Michigan 48109-1040, United States*

(Dated: September 26, 2024)

We investigate microwave interference from a spin ensemble and its mirror image in a one-dimensional waveguide. Away from the mirror, the resonance frequencies of the Kittel mode (KM) inside a ferrimagnetic spin ensemble have sinusoidal shifts as the normalized distance between the spin ensemble and the mirror increases compared to the setup without the mirror. These shifts are a consequence of the KM's interaction with its own image. Furthermore, the variation of the magnon radiative decay into the waveguide shows a cosine squared oscillation and is enhanced twofold when the KM sits at the magnetic antinode of the corresponding eigenmode. We can finely tune the KM to achieve the maximum adsorption of the input photons at the critical coupling point. Moreover, by placing the KM in proximity to the node of the resonance field, its *lifetime is extended to more than eight times* compared to its positioning near the antinode.

Introduction.—Recent studies on spin ensembles have utilized light-matter interaction [1, 2] through collective effects for coherent information processing in both the quantum and classical regimes [3, 4]. Significant advances have been made in cavity magnonics [5], demonstrating (ultra) strong coupling between a magnon mode and a cavity mode [6–13], information transduction [14–16], bistability [17–19], exceptional points [20, 21], memory applications [22, 23], and proposing the generation of entangled quantum states between magnons, cavity photons and phonons [24, 25], as well as magnon squeezed states [26]. Additionally, coupling between magnons and a superconducting qubit, mediated by cavity photons, has been achieved [27–30]. Beyond single modes, coherence transfer through continuous photonic modes have been investigated in waveguide magnonics [31–34], opening up avenues for studying giant atom physics [32] and developing non-Hermitian physics [33].

Since Purcell's seminal work [35], the implementation of a simple "cavity" boundary with a single mirror has supported a fully open system with continuous photonic modes. This configuration allows for the engineering of electromagnetic field modes around an atom [36, 37], thereby modifying its emission properties through mirror-induced interference. For example, the fluorescence of a single Ba^+ ion near a floating mirror is either enhanced or reduced due to the interaction between the ion and its mirror image via optically radiative means [38]. In another instance, a superconducting artificial atom (transmon)-mirror system demonstrated that, using a mirror, the device enables the detection of the spectral density of vacuum fluctuations [39], the study of Landau-Zener-Stückelberg-Majorana interferometry [40–42], and the deterministic loading of microwaves [43]. More importantly, mirror-shaped photonic modes can shift energy levels through virtual photon processes [44, 45]. For example, in a three-dimensional (3D) single atom far from a mirror [46], the level shifts are approximately of $\pm 150\,\mathrm{kHz}$, a value that is limited due to the small effective solid angle. In a 1D geometry, implemented by coupling the artificial atom to a semi-infinite waveguide, theoretical predictions show that the energy shifts vary periodically through effectively altering the atom-mirror distance [47]. However, such an energy level shift and its relation to radiative decay have not been observed in this 1D setup due to the absence of a reference setup [39]. Additionally, controlling the atom's lifetime in such configuration in the time domain is still unexplored.

In this work, we use a Yttrium Iron Garnet (YIG, $Y_3Fe_5O_{12}$) sphere as an ideal spin ensemble with a high spin density $2.1 \times 10^{22} \mu_B\,\mathrm{cm}^{-3}$ (μ_B: Bohr magneton) [48, 49] and low intrinsic loss [6, 7], to explore *mirror induced interference effects*. By applying an external

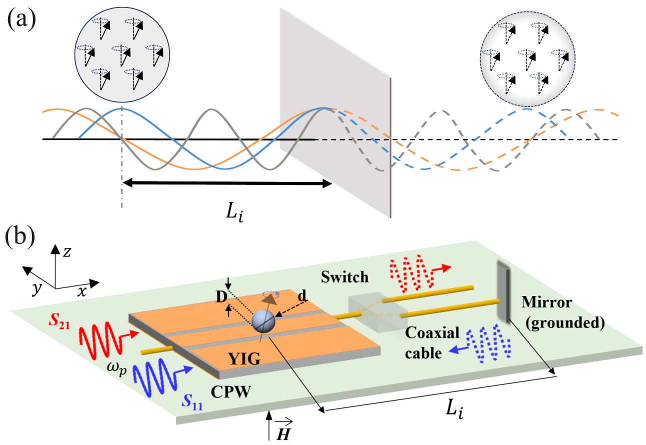

Figure 1. Schematic of the system and experimental setup. (a) A YIG sphere is positioned at a distance L_i from the mirror. The three color curves show the mode structures of the propagating magnetic field. The coupling between the magnetic field (orange) and the KM is minimal when the KM sits at the node (vertical dashed line) of the propagating resonant field. (b) The experimental setup is composed of a YIG sphere with a diameter d being placed above the CPW plane at a height D. In the grounded mirror system, a short load is used as the mirror to reflect the microwave at the end of the path. By measuring the reflection coefficient S_{11} (blue waves), the mirror-induced interference effects can be probed and analyzed. The system without the mirror is considered as a reference, characterized by measuring the transmission coefficient S_{21} (red waves).

magnetic field, the magnon modes (dipolar spin waves or magnetostatic modes) of this YIG can be detected through microwave excitation. These magnon modes, arising from the collective behaviour of electron spins, exhibiting bosonic characteristics [50]. In this work, we focus on investigating the interference between a particular magnon mode, the Kittel mode (KM), and its mirror image in a 1D geometry [see Fig. 1(a)], where the precession of spins is in phase [51]. This setup [52–60] *enhances interactions and reduces the decay into unwanted modes compared to the 3D cases* [38]. To observe the KM resonance shifts, we construct two systems, one with a grounded mirror and one without, which can be selected by a microwave switch [see Fig. 1(b)]. By tuning the KM frequency, we demonstrate that the continuous resonance shifts vary periodically over a full wavelength. The maximum shift depends on the round trip phase and the YIG size. Additionally, with the mirror, the excited KM interferes with its own radiation, causing a change in the radiative decay, which is enhanced at the antinodes and diminished at nodes under the corresponding eigenmodes, thereby altering the KM's lifetime. This modification enables the formation of *controllable ultra-sharp adsorption dips*.

System and model.—Our experimental setup, shown in Fig. 1(b), consists of a YIG sphere placed on top of a coplanar waveguide (CPW). We can extensively tune the KM or other magnon modes at room temperature. The KM, regarded as having a large magnetic dipole moment [6, 7], enables strong magnon-photon coupling. In the system with a mirror, the coherent input interacts with the KM and continues propagating towards the mirror. When the KM is excited, the emitted field is evenly distributed between the left- and right-moving fields. Both the input and the right-moving field are reflected by the mirror and subsequently interfere with the left-moving field. Notably, a round trip time or a delay time is much smaller ($2L_i/\nu \approx 2 \sim 5\,\mathrm{ns}$) compared to the lifetime of the KM ($\approx 70\,\mathrm{ns}$). Therefore, the magnon-photon interaction for this feedback-included system occurs in a Markovian regime [61]. Here, $L_i \approx 21 \sim 53\,\mathrm{cm}$ represents the distance between the YIG sphere and the mirror, where in this work we have four different distances ($i = 1, 2, 3, 4$), and $\nu \approx 2.1 \times 10^8\,\mathrm{m/s}$ denotes the speed of the light (Section S2 in [62]).

The phase resulting from the round trip is given by (Eq. (S9) [62])

$$\theta(I) = 2 \times 2\pi L_i/\lambda(I), \tag{1}$$

where $\lambda(I) = 2\pi\nu/\omega_{m,t}(I)$ is the wavelength of the KM transition frequency $\omega_{m,t}$ without considering the mirror effect and I denotes the current passing through the electromagnet. The subscripts t (transmission) and r (reflection) refer to the cases without and with the mirror, respectively. Furthermore, due to the presence of the mirror, the radiative damping rate κ_r and the resonant shift $\delta\omega \equiv \omega_{m,r} - \omega_{m,t}$ can be related to the phase $\theta(I)$ through:

$$\kappa_r = (2\kappa_b)\cos^2[\theta(I)/2] \tag{2}$$

and

$$\delta\omega = (\kappa_b/2)\sin[\theta(I)], \tag{3}$$

respectively (Eqs. (S7,S8) [62]). Here κ_b denotes the bare radiative damping rate.

Results and discussions.—To investigate the interference effects, we adjust the distance L_i by varying the length of the coaxial cable. Initially, we set $L_1 = 22.8\,\mathrm{cm}$ (see section S2 [62]) and use a YIG sphere with a diameter $d = 1.0\,\mathrm{mm}$. We introduce a tunable static magnetic field $\vec{H}$ adjusted by the applied current I, which is perpendicular to the CPW plane and to the YIG's crystal axis <110>, to control the magnon resonance frequency [see Fig. 1(b)]. The sample is assumed to be uniformly magnetized. We characterize the system by measuring the reflection coefficient S_{11} in the mirror setup and the transmission coefficient S_{21} in the reference setup without the mirror. The probe power is set to $-30\,\mathrm{dBm}$ to ensure the KM's excitation remained in the linear regime.

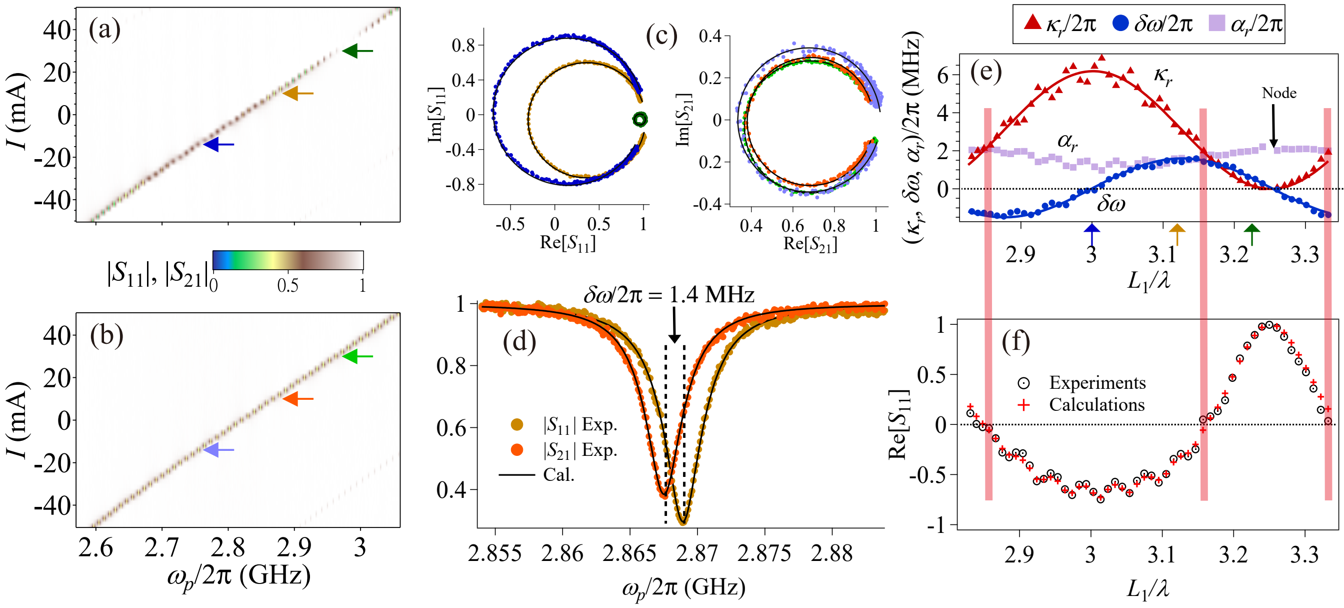

Figure 2. Spectroscopy of the YIG sphere with diameter $d = 1.0\,\mathrm{mm}$. (a) Reflection spectrum $|S_{11}|$ versus the current I for the YIG-mirror system. (b) Transmission spectrum $|S_{21}|$ against the current I for the system *without* the mirror. In addition to the Kittel mode to be probed, a high-order magnetostatic mode is observed in the lower right corner of (a) and (b). (c) In-phase-and-Quadrature (IQ) plots for the reflection and transmission spectra. The left and right panels display complex plane representations of the reflection and transmission coefficients ($[S_{11}]$ and $[S_{21}]$) for three different resonance frequencies of this YIG, as indicated by the horizontal arrows in (a). In this representation, the coefficient $[S_{11}]$ and $[S_{21}]$ form circles, with the diameter of these circles corresponding to the KM's linewidth $\Gamma_{r(t)}$. Without special instructions, symbols are experimental data. Here, the solid curves follow Eqs. (4,5). The extracted parameters are given in Table. I. (d) The line-cut plot for both reflection and transmission spectra for the current $I = 8\,\mathrm{mA}$. (e) The radiative damping rate $\kappa_r/2\pi$ (red triangles), resonant shifts $\delta\omega/2\pi$ (blue dots), and non-radiative damping rate $\alpha_r/2\pi$ (purple squares) versus the normalized distance, L_1/λ, with $\lambda = \nu/(\omega_{m.t}/2\pi)$ being the resonant wavelength, for the KM of a YIG away from the mirror. Here, the red (blue) solid curve is based on Eq. (2) [Eq. (3)]. The short vertical arrows on the bottom axis in (e) correspond to the three horizontal arrows shown in (a). (f) Real part of the reflection $[S_{11}]$ as a function of the effective distance L_1/λ. The critical coupling points are indicated by the red faint lines, which are formed when $\kappa_r = \alpha_r$, and $\omega_p = \omega_{\mathrm{m,r}}$.

	$\omega_{m,r}/2\pi$	$\kappa_r/2\pi$	$\Gamma_r/2\pi$	$\alpha_r/2\pi$		$\omega_{m,t}/2\pi$	$\kappa_t/2\pi$	$\Gamma_t/2\pi$	$\alpha_t/2\pi$
	GHz	MHz	MHz	MHz		GHz	MHz	MHz	MHz
→	2.7549	6.434	3.797	1.160	→	2.7551	3.291	2.438	1.585
→	2.8689	2.969	2.291	1.613	→	2.8675	2.614	2.124	1.634
→	2.9628	0.131	1.070	2.009	→	2.9623	3.063	2.442	1.821

Table I. Summary of the Kittel mode parameters indicated by the six horizontal color arrows in Figs. 2(a,b).

In the steady state, the reflection and transmission coefficients are given by (Eqs. (S11,S20) [62]):

$$S_{11} = 1 - \frac{\kappa_r}{\Gamma_r - i(\omega_p - \omega_{m,r})} \tag{4}$$

and

$$S_{21} = 1 - \frac{\kappa_t/2}{\Gamma_t - i(\omega_p - \omega_{m,t})}, \tag{5}$$

where $\Gamma_{r(t)} = (\kappa_{r(t)} + \alpha_{r(t)})/2$, with $\alpha_{r(t)}$ denoting the non-radiative decay, represents the overall damping rate (linewidth) of the KM.

In Figs. 2(a,b) we plot the reflection and transmission spectra as a function of the applied current I. We find that the absorption dips occur at the probe frequencies ω_p equal to the KM resonance frequencies $\omega_{m,r(t)}$, allowing us to here focus only on the KM. When $I = 0$, the external permanent magnet and the internal anisotropy field of the YIG sphere contribute to $\omega_{m,t}/2\pi = 2.8204\,\mathrm{GHz}$. To analyze the KM behavior, we examine the spectroscopic line shape. Near the resonant dips indicated by arrows in Figs. 2(a,b), the complex plane representations of S_{21} and S_{11} manifest themselves as circles [63], as shown in Fig. 2(c), with the diameter of these circles corresponding to the KM's linewidth $\Gamma_{r(t)}$. Smaller diameters indicate weaker magnon-photon coupling. By using Eqs. (4,5), we can extract $\kappa_{r(t)}, \Gamma_{r(t)}, \omega_{m,r(t)}$, and $\alpha_{r(t)}$ (see Table. I). When $\omega_{m,r}/2\pi$ is around 2.9628 GHz, the coupling strength approaches zero, inhibiting real photon exchange [64, 65]. This occurs when the KM is located at the magnetic node of the corresponding eigenmode, effectively concealing itself from the probe field. In the reference setup, the radiative damping κ_t remains in the same order of magnitude ($\kappa_t/2\pi \approx 3$ MHz) for these three cases.

We then show the extracted $\kappa_r/2\pi$ (red triangles) versus distance L_1/λ in Fig. 2(e) by fitting all spectra shown in Fig. 2(a). We first observe that the theoretical calculation, using Eqs. (1,2), aligns well with our measurement, allowing us to extract the bare damping rate $\kappa_b/2\pi = 3.092$ MHz. When the normalized distance is near $L_1/\lambda = 3.25$, $\kappa_r/2\pi$ approaches zero, signaling that the KM is at the node of its eigenmode. However, when $L_1/\lambda = 3$, we observe $\kappa_r/2\pi = 6.434$ MHz which is nearly twice that of the same I, where $\kappa_t/2\pi = 3.291$ MHz, suggesting that the waveguide-magnon coupling is enhanced by putting the YIG at the antinode of its eigenmode.

Furthermore, the interaction between the KM and its mirror image causes energy-level shifts. We then demonstrate this from the reflection and transmission spectra when $I = 8$ mA, as shown in Fig. 2(d). We observe that the resonance frequency shift $\delta\omega = \omega_{m,r} - \omega_{m,t} = 2\pi \times 1.4$ MHz, after correcting for impedance mismatch [63]. To further study this shift, we measure the resonance frequency shift $\delta\omega$ against the distance L_1/λ, as depicted in Fig. 2(e). Our theoretical calculations, using Eqs. (1,3), fit the experimental data well, validating the *self-interaction* of the YIG and its image, resulting in peak-to-peak frequency shifts of approximately $\kappa_b/2 = 2\pi \times \pm 1.54$ MHz. Interestingly, when $L_1/\lambda = 3$, the resonance frequency shift vanishes ($\delta\omega = 0$), even with maximum magnon-photon coupling. This is attributed to the accumulated phase $\theta(I)$ at the antinode being an integer multiple of π, according to Eqs. (1,2,3). We also notice that the maximum resonant shift occurs at the midpoint between the antinode and node, and the position-dependent shift can be either negative or positive.

In Fig. 2(f) we show the real part of the reflection coefficient S_{11} versus the distance L_1/λ in the resonant case when $\omega_p = \omega_{m,r}$. Note that, in this plot, the imaginary part of S_{11} is close to zero. Negative Re[S_{11}], resulting from the π phase shift in the output voltage, indicates strong coupling between the YIG and resonant microwave. According to Eq. (4) we find that the value of Re[S_{11}] depends on the magnitude ratio between κ_r and Γ_r. We observe Re[S_{11}] = 0, indicative of all the coherent input photons that lose their energy, forming an ultrasharp adsorption dip [see an example in Fig. S4(a) [62] that reaches −49.7 dB]. This satisfies the critical coupling condition [47, 66, 67], requiring $\kappa_r = \alpha_r$, indicated by the red faint lines connecting Figs. 2(e) and 2(f). By adjusting the distance from L_2 (38.1 cm) to L_3 (53.3 cm), the critical coupling points are shifted and increased [see Section S3 [62]], aligning with the predicted periods of κ_r and $\delta\omega$. This observation validates the theoretical predictions through Eqs. (2,3).

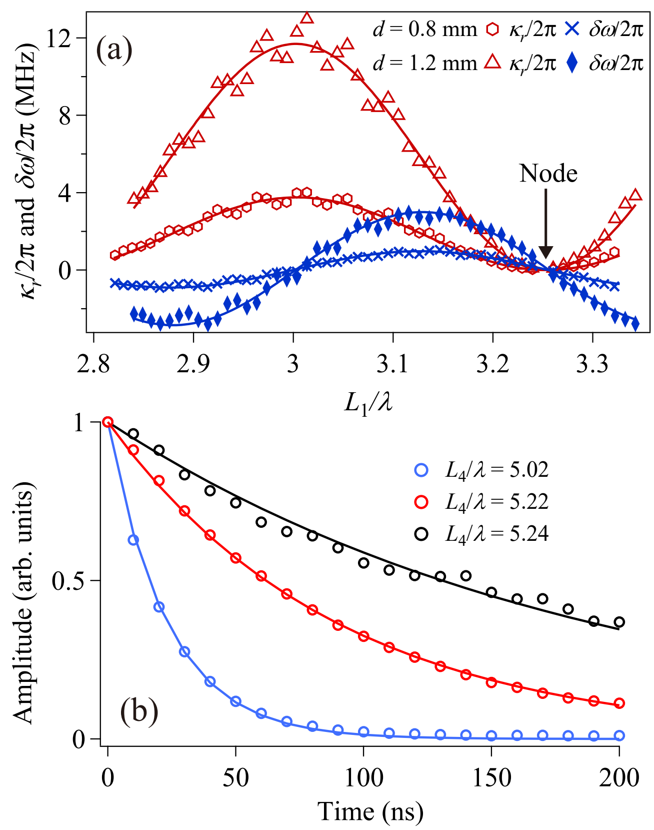

Figure 3. Collective coupling and temporal dynamic emission. (a) The variations of the radiative damping rate $\kappa_r/2\pi$ and the resonance shifts $\delta\omega/2\pi$ of the KM with the effective distance L_1/λ for YIG spheres with different diameters $d = 0.8, 1.2$ mm. Here, symbols are experimental data that are obtained from the same setup in Fig. 1. The red (blue) theoretical curves in (a) is based on Eq. (2) (Eq. (3)) with $\kappa_b/2\pi = 5.845$ MHz for $d = 1.2$ mm ($\kappa_b/2\pi = 1.946$ MHz for $d = 0.8$ mm). (b) The temporal dynamics of the excited KM of the YIG sphere with $d = 1.2$ mm when it sits at L_4/λ [see Fig. S5 [62] for details]. The circles represent the experimental data. The solid curves are fitted by the exponential function, which gives lifetimes: 23.1 ± 0.1 ns (blue), 89.0 ± 0.2 ns (red), and 188.4 ± 12.1 ns (black). The experimental setup is shown in Fig. S1(b) [62].

We now turn to investigate the dependence of κ_r and $\delta\omega$ on the size of the YIG sphere, which directly correlates with the number of spins. Figure 3(a) shows an enhancement in the interference fringe amplitude for the large sphere ($d = 1.2$ mm) with $\kappa_b/2\pi = 5.845$ MHz (see Table. S1 for details [62]). This proves that increasing the number of spins leads to an *enhanced collective* *effect and a stronger resonant dipole-dipole interaction with its mirror image*. Moreover, the spatial distribution of the field in the CPW also affects κ_t [68, 69]. When the height D (see Fig. 1) is larger than d, κ_t is proportional to the number of spins (see Fig. S6(b) [62]). We further characterize the grounded mirror system in the time domain with a YIG sphere of $d = 1.2\,\mathrm{mm}$ using a square pulse excitation. After the resonant pulse excites the KM, an exponential decay of the photon energy is observed, as shown in Fig. 3(b). For the case where $L_4/\lambda = 5.02$ and $\omega_{m,r}/2\pi = 3.008\,\mathrm{GHz}$, the magnon lifetime $\tau = 23.1 \pm 0.1\,\mathrm{ns}$ is obtained by directly fitting the experimental data with an exponential function, in agreement with the frequency domain result via $\tau = 1/\Gamma_r = 23.0\,\mathrm{ns}$ with $\Gamma_r/2\pi = 6.919\,\mathrm{MHz}$. The lifetime of the KM located near the node ($L_4/\lambda = 5.24$) is $\tau = 188.4 \pm 12.1\,\mathrm{ns}$, although its output emission is very weak [see Fig. S5(b) [62]]. *The lifetime near the node is more than eight times longer than that near the antinode*. These results demonstrate our ability to *finely control the magnon lifetime, leading to either reduced or enhanced emission*, all achieved without physically moving the sphere.

Summary and outlook.—In the mirror-embedded 1D waveguide magnonic system, the KM exhibits sinusoidal resonant shifts and radiative damping oscillations due to its interference with its own radiation. These results arise from the coupling to continuous photonic modes. Consequently, we are empowered to perform precise and continuous tuning of the real photon exchange processes, ranging from maximal coupling to decoupling between the KM and photons. This gives us control over the formation of critical couplings, characterized by the perfect adsorption. Finally, the ability to control the lifetime of magnons provides a valuable tool for coherent information processing.

Acknowledgements.—I.-C.H. acknowledges financial support from City University of Hong Kong through the start-up project 9610569, from the Research Grants Council of Hong Kong (Grant No. 11312322) and from Guangdong Provincial Quantum Science Strategic Initiative (GDZX2303005 and GDZX2200001). F.N. is supported in part by: Nippon Telegraph and Telephone Corporation (NTT) Research, the Japan Science and Technology Agency (JST) [via the Quantum Leap Flagship Program (Q-LEAP), and the Moonshot R&D Grant Number JPMJMS2061], and the Office of Naval Research (ONR) Global (via Grant No. N62909-23-1-2074).

* These authors contributed equally
† e-mail:iochoi@cityu.edu.hk

[1] M. O. Scully and M. S. Zubairy, *Quantum Optics* (Cambridge University Press, 1997).
[2] G. S. Agarwal, *Quantum Optics* (Cambridge University Press, 2012).
[3] M. D. Lukin, Colloquium: Trapping and manipulating photon states in atomic ensembles, Rev. Mod. Phys. **75**, 457 (2003).
[4] A. Imamoğlu, Cavity QED based on collective magnetic dipole coupling: Spin ensembles as hybrid two-level systems, Phys. Rev. Lett. **102**, 083602 (2009).
[5] B. Zare Rameshti, S. Viola Kusminskiy, J. A. Haigh, K. Usami, D. Lachance-Quirion, Y. Nakamura, C.-M. Hu, H. X. Tang, G. E. Bauer, and Y. M. Blanter, Cavity magnonics, Physics Reports **979**, 1 (2022), cavity Magnonics.
[6] Y. Tabuchi, S. Ishino, T. Ishikawa, R. Yamazaki, K. Usami, and Y. Nakamura, Hybridizing ferromagnetic magnons and microwave photons in the quantum limit, Phys. Rev. Lett. **113**, 083603 (2014).
[7] X. Zhang, C.-L. Zou, L. Jiang, and H. X. Tang, Strongly coupled magnons and cavity microwave photons, Phys. Rev. Lett. **113**, 156401 (2014).
[8] M. Goryachev, W. G. Farr, D. L. Creedon, Y. Fan, M. Kostylev, and M. E. Tobar, High-cooperativity cavity QED with magnons at microwave frequencies, Phys. Rev. Appl. **2**, 054002 (2014).
[9] D. Zhang, X.-M. Wang, T.-F. Li, X.-Q. Luo, W. Wu, F. Nori, and J. Q. You, Cavity quantum electrodynamics with ferromagnetic magnons in a small Yttrium-iron-garnet sphere, npj Quantum Information **1**, 15014 (2015).
[10] J. Bourhill, N. Kostylev, M. Goryachev, D. L. Creedon, and M. E. Tobar, Ultrahigh cooperativity interactions between magnons and resonant photons in a YIG sphere, Phys. Rev. B **93**, 144420 (2016).
[11] N. Kostylev, M. Goryachev, and M. E. Tobar, Superstrong coupling of a microwave cavity to Yttrium iron garnet magnons, Applied Physics Letters **108**, 062402 (2016).
[12] M. Goryachev, S. Watt, J. Bourhill, M. Kostylev, and M. E. Tobar, Cavity magnon polaritons with lithium ferrite and three-dimensional microwave resonators at millikelvin temperatures, Phys. Rev. B **97**, 155129 (2018).
[13] G. Flower, M. Goryachev, J. Bourhill, and M. E. Tobar, Experimental implementations of cavity-magnon systems: from ultra strong coupling to applications in precision measurement, New Journal of Physics **21**, 095004 (2019).
[14] X. Zhang, C.-L. Zou, L. Jiang, and H. X. Tang, Cavity magnomechanics, Science Advances **2**, e1501286 (2016).
[15] R. Hisatomi, A. Osada, Y. Tabuchi, T. Ishikawa, A. Noguchi, R. Yamazaki, K. Usami, and Y. Nakamura, Bidirectional conversion between microwave and light via ferromagnetic magnons, Phys. Rev. B **93**, 174427 (2016).
[16] A. Osada, R. Hisatomi, A. Noguchi, Y. Tabuchi, R. Yamazaki, K. Usami, M. Sadgrove, R. Yalla, M. Nomura, and Y. Nakamura, Cavity optomagnonics with spin-orbit coupled photons, Phys. Rev. Lett. **116**, 223601 (2016).
[17] Y.-P. Wang, G.-Q. Zhang, D. Zhang, T.-F. Li, C.-M. Hu, and J. Q. You, Bistability of cavity magnon polaritons, Phys. Rev. Lett. **120**, 057202 (2018).
[18] J. M. P. Nair, D. Mukhopadhyay, and G. S. Agarwal, Ultralow threshold bistability and generation of long-lived mode in a dissipatively coupled nonlinear system: Application to magnonics, Phys. Rev. B **103**, 224401 (2021).
[19] R.-C. Shen, J. Li, Z.-Y. Fan, Y.-P. Wang, and J. Q. You, Mechanical bistability in Kerr-modified cavity magnomechanics, Phys. Rev. Lett. **129**, 123601 (2022).

[20] D. Zhang, X.-Q. Luo, Y.-P. Wang, T.-F. Li, and J. Q. You, Observation of the exceptional point in cavity magnon-polaritons, Nature Communications **8**, 1368 (2017).

[21] G.-Q. Zhang and J. Q. You, Higher-order exceptional point in a cavity magnonics system, Phys. Rev. B **99**, 054404 (2019).

[22] X. Zhang, C.-L. Zou, N. Zhu, F. Marquardt, L. Jiang, and H. X. Tang, Magnon dark modes and gradient memory, Nature Communications **6**, 8914 (2015).

[23] R.-C. Shen, Y.-P. Wang, J. Li, S.-Y. Zhu, G. S. Agarwal, and J. Q. You, Long-time memory and ternary logic gate using a multistable cavity magnonic system, Phys. Rev. Lett. **127**, 183202 (2021).

[24] J. Li, S.-Y. Zhu, and G. S. Agarwal, Magnon-photon-phonon entanglement in cavity magnomechanics, Phys. Rev. Lett. **121**, 203601 (2018).

[25] Z. Zhang, M. O. Scully, and G. S. Agarwal, Quantum entanglement between two magnon modes via Kerr nonlinearity driven far from equilibrium, Phys. Rev. Res. **1**, 023021 (2019).

[26] J. Li, S.-Y. Zhu, and G. S. Agarwal, Squeezed states of magnons and phonons in cavity magnomechanics, Phys. Rev. A **99**, 021801 (2019).

[27] Y. Tabuchi, S. Ishino, A. Noguchi, T. Ishikawa, R. Yamazaki, K. Usami, and Y. Nakamura, Coherent coupling between a ferromagnetic magnon and a superconducting qubit, Science **349**, 405 (2015).

[28] D. Lachance-Quirion, Y. Tabuchi, S. Ishino, A. Noguchi, T. Ishikawa, R. Yamazaki, and Y. Nakamura, Resolving quanta of collective spin excitations in a millimeter-sized ferromagnet, Science Advances **3**, e1603150 (2017).

[29] D. Lachance-Quirion, S. P. Wolski, Y. Tabuchi, S. Kono, K. Usami, and Y. Nakamura, Entanglement-based single-shot detection of a single magnon with a superconducting qubit, Science **367**, 425 (2020).

[30] D. Xu, X.-K. Gu, H.-K. Li, Y.-C. Weng, Y.-P. Wang, J. Li, H. Wang, S.-Y. Zhu, and J. Q. You, Quantum control of a single magnon in a macroscopic spin system, Phys. Rev. Lett. **130**, 193603 (2023).

[31] J. W. Rao, Y. P. Wang, Y. Yang, T. Yu, Y. S. Gui, X. L. Fan, D. S. Xue, and C.-M. Hu, Interactions between a magnon mode and a cavity photon mode mediated by traveling photons, Phys. Rev. B **101**, 064404 (2020).

[32] Z.-Q. Wang, Y.-P. Wang, J. Yao, R.-C. Shen, W.-J. Wu, J. Qian, J. Li, S.-Y. Zhu, and J. Q. You, Giant spin ensembles in waveguide magnonics, Nature Communications **13**, 7580 (2022).

[33] J. Qian, C. H. Meng, J. W. Rao, Z. J. Rao, Z. An, Y. Gui, and C.-M. Hu, Non-Hermitian control between absorption and transparency in perfect zero-reflection magnonics, Nature Communications **14**, 3437 (2023).

[34] C. Wang, J. Rao, Z. Chen, K. Zhao, L. Sun, B. Yao, T. Yu, Y.-P. Wang, and W. Lu, Enhancement of magnonic frequency combs by exceptional points, Nature Physics **20**, 1139 (2024).

[35] E. M. Purcell, H. C. Torrey, and R. V. Pound, Resonance absorption by nuclear magnetic moments in a solid, Phys. Rev. **69**, 37 (1946).

[36] I. Buluta and F. Nori, Quantum simulators, Science **326**, 108 (2009).

[37] I. M. Georgescu, S. Ashhab, and F. Nori, Quantum simulation, Rev. Mod. Phys. **86**, 153 (2014).

[38] J. Eschner, C. Raab, F. Schmidt-Kaler, and R. Blatt, Light interference from single atoms and their mirror images, Nature **413**, 495 (2001).

[39] I.-C. Hoi, A. F. Kockum, L. Tornberg, A. Pourkabirian, G. Johansson, P. Delsing, and C. M. Wilson, Probing the quantum vacuum with an artificial atom in front of a mirror, Nature Physics **11**, 1045 (2015).

[40] S. Shevchenko, S. Ashhab, and F. Nori, Landau-Zener-Stückelberg interferometry, Physics Reports **492**, 1 (2010).

[41] P. Y. Wen, O. V. Ivakhnenko, M. A. Nakonechnyi, B. Suri, J.-J. Lin, W.-J. Lin, J. C. Chen, S. N. Shevchenko, F. Nori, and I.-C. Hoi, Landau-Zener-Stückelberg-Majorana interferometry of a superconducting qubit in front of a mirror, Phys. Rev. B **102**, 075448 (2020).

[42] M. P. Liul, C.-H. Chien, C.-Y. Chen, P. Y. Wen, J. C. Chen, Y.-H. Lin, S. N. Shevchenko, F. Nori, and I.-C. Hoi, Coherent dynamics of a photon-dressed qubit, Phys. Rev. B **107**, 195441 (2023).

[43] W.-J. Lin, Y. Lu, P. Y. Wen, Y.-T. Cheng, C.-P. Lee, K. T. Lin, K. H. Chiang, M. C. Hsieh, C.-Y. Chen, C.-H. Chien, J. J. Lin, J.-C. Chen, Y. H. Lin, C.-S. Chuu, F. Nori, A. Frisk Kockum, G. D. Lin, P. Delsing, and I.-C. Hoi, Deterministic loading of microwaves onto an artificial atom using a time-reversed waveform, Nano Letters **22**, 8137 (2022).

[44] D. Meschede, W. Jhe, and E. A. Hinds, Radiative properties of atoms near a conducting plane: An old problem in a new light, Phys. Rev. A **41**, 1587 (1990).

[45] U. Dorner and P. Zoller, Laser-driven atoms in half-cavities, Phys. Rev. A **66**, 023816 (2002).

[46] M. A. Wilson, P. Bushev, J. Eschner, F. Schmidt-Kaler, C. Becher, R. Blatt, and U. Dorner, Vacuum-field level shifts in a single trapped ion mediated by a single distant mirror, Phys. Rev. Lett. **91**, 213602 (2003).

[47] K. Koshino and Y. Nakamura, Control of the radiative level shift and linewidth of a superconducting artificial atom through a variable boundary condition, New Journal of Physics **14**, 043005 (2012).

[48] M. A. Gilleo and S. Geller, Magnetic and crystallographic properties of substituted Yttrium-Iron Garnet, $3\mathrm{Y_2O_3} \cdot \mathrm{xM_2O_3} \cdot (5-\mathrm{x})\mathrm{Fe_2O_3}$, Phys. Rev. **110**, 73 (1958).

[49] H. Huebl, C. W. Zollitsch, J. Lotze, F. Hocke, M. Greifenstein, A. Marx, R. Gross, and S. T. B. Goennenwein, High cooperativity in coupled microwave resonator ferrimagnetic insulator hybrids, Phys. Rev. Lett. **111**, 127003 (2013).

[50] D. Stancil and A. Prabhakar, *Spin Waves: Theory and Applications* (Springer US, 2009).

[51] R. H. Dicke, Coherence in spontaneous radiation processes, Phys. Rev. **93**, 99 (1954).

[52] O. Astafiev, A. M. Zagoskin, A. A. Abdumalikov, Y. A. Pashkin, T. Yamamoto, K. Inomata, Y. Nakamura, and J. S. Tsai, Resonance fluorescence of a single artificial atom, Science **327**, 840 (2010).

[53] J. Q. You and F. Nori, Atomic physics and quantum optics using superconducting circuits, Nature **474**, 589 (2011).

[54] I.-C. Hoi, C. M. Wilson, G. Johansson, T. Palomaki, B. Peropadre, and P. Delsing, Demonstration of a single-photon router in the microwave regime, Phys. Rev. Lett. **107**, 073601 (2011).

[55] I.-C. Hoi, T. Palomaki, J. Lindkvist, G. Johansson, P. Delsing, and C. M. Wilson, Generation of nonclassi-

cal microwave states using an artificial atom in 1D open space, Phys. Rev. Lett. **108**, 263601 (2012).

[56] I.-C. Hoi, A. F. Kockum, T. Palomaki, T. M. Stace, B. Fan, L. Tornberg, S. R. Sathyamoorthy, G. Johansson, P. Delsing, and C. M. Wilson, Giant cross–Kerr effect for propagating microwaves induced by an artificial atom, Phys. Rev. Lett. **111**, 053601 (2013).

[57] X. Gu, A. F. Kockum, A. Miranowicz, Y. X. Liu, and F. Nori, Microwave photonics with superconducting quantum circuits, Physics Reports **718-719**, 1 (2017).

[58] A. F. Kockum and F. Nori, Quantum Bits with Josephson Junctions, in *Springer Series in Materials Science* (Springer International Publishing, 2019).

[59] P. Y. Wen, A. F. Kockum, H. Ian, J. C. Chen, F. Nori, and I.-C. Hoi, Reflective amplification without population inversion from a strongly driven superconducting qubit, Phys. Rev. Lett. **120**, 063603 (2018).

[60] P. Y. Wen, K.-T. Lin, A. F. Kockum, B. Suri, H. Ian, J. C. Chen, S. Y. Mao, C. C. Chiu, P. Delsing, F. Nori, G.-D. Lin, and I.-C. Hoi, Large collective Lamb shift of two distant superconducting artificial atoms, Phys. Rev. Lett. **123**, 233602 (2019).

[61] G. Crowder, L. Ramunno, and S. Hughes, Quantum trajectory theory and simulations of nonlinear spectra and multiphoton effects in waveguide-QED systems with a time-delayed coherent feedback, Phys. Rev. A **106**, 013714 (2022).

[62] See supplemental material for details on the experimental setup, YIG-mirror distance calibration, additional figures of Kittel mode in frequency and time-domain measurements, the dependence of collective coupling on both the height (D) and the YIG size (d), and the theory of magnons in a semi-infinite waveguide and open waveguides.

[63] S. Probst, F. B. Song, P. A. Bushev, A. V. Ustinov, and M. Weides, Efficient and robust analysis of complex scattering data under noise in microwave resonators, Review of Scientific Instruments **86**, 024706 (2015).

[64] A. F. Kockum, G. Johansson, and F. Nori, Decoherence-free interaction between giant atoms in waveguide quantum electrodynamics, Phys. Rev. Lett. **120**, 140404 (2018).

[65] B. Kannan, M. J. Ruckriegel, D. L. Campbell, A. Frisk Kockum, J. Braumüller, D. K. Kim, M. Kjaergaard, P. Krantz, A. Melville, B. M. Niedzielski, A. Vepsäläinen, R. Winik, J. L. Yoder, F. Nori, T. P. Orlando, S. Gustavsson, and W. D. Oliver, Waveguide quantum electrodynamics with superconducting artificial giant atoms, Nature **583**, 775 (2020).

[66] M. L. Gorodetsky and V. S. Ilchenko, Optical microsphere resonators: optimal coupling to high-Q whispering-gallery modes, J. Opt. Soc. Am. B **16**, 147 (1999).

[67] M. Cai, O. Painter, and K. J. Vahala, Observation of critical coupling in a fiber taper to a silica-microsphere whispering-gallery mode system, Phys. Rev. Lett. **85**, 74 (2000).

[68] J. W. Rao, S. Kaur, X. L. Fan, D. S. Xue, B. M. Yao, Y. S. Gui, and C.-M. Hu, Characterization of the non-resonant radiation damping in coupled cavity photon magnon system, Applied Physics Letters **110**, 262404 (2017).

[69] Y. Yang, M. Harder, J. W. Rao, B. M. Yao, W. Lu, Y. S. Gui, and C.-M. Hu, Influence of stripline coupling on the magnetostatic mode line width of an Yttrium-iron-garnet sphere, AIP Advances **8**, 075315 (2018).